Journal of Power Sources 240 (2013) 8–13

Contents lists available at SciVerse ScienceDirect

Journal of Power Sources

journal homepage: www.elsevier.com/locate/jpowsour

Efficient electron injection in non-toxic silver sulfide (Ag_2S) sensitized solar cells

Heping Shen [a,1], Xingjian Jiao [a,1], Dan Oron [b], Jianbao Li [c], Hong Lin [a,*]

[a] State Key Laboratory of New Ceramics and Fine Processing, School of Materials Science and Engineering, Tsinghua University, Beijing 100084, PR China
[b] Department of Physics of Complex Systems, Weizmann Institute of Science, Rehovot 76100, Israel
[c] College of Materials Science and Chemical Engineering, Hainan University, Haikou 570228, PR China

HIGHLIGHTS

- α-Ag_2S serves as a promising candidate for non-toxic solar cell.
- The energy level alignment between metal oxide and sensitizer is vital.
- ~0.6 eV CB offset for SnO_2/Ag_2S supplied a sufficient injection driving force.
- An impressive current density for SnO_2/Ag_2S based solar cell was obtained.

ARTICLE INFO

Article history:
Received 5 February 2013
Received in revised form
25 March 2013
Accepted 29 March 2013
Available online 9 April 2013

Keywords:
Non-toxic
Silver sulfide
Conduction band offset
Semiconductor sensitized solar cell
Electron injection

ABSTRACT

α-Ag_2S, with a direct forbidden bandgap of about 1.0 eV, is a non-toxic low bandgap semiconductor which can readily be deposited in the form of a thin film by chemical bath deposition. In a solar cell configuration, it can potentially provide a high short-circuit current due to the infrared absorption, and is compatible with the polysulfide electrolyte. Its practical use in a solar cell depends, however, critically on band alignment between the Ag_2S, the oxide anode and the electrolyte redox potential. Here we examine the conduction band (CB) offsets in the nanostructured α-Ag_2S sensitized TiO_2 and SnO_2 electrodes by X-ray Photoelectron Spectroscopy, and show that they can significantly differ from the extrapolated bulk values. The much higher CB offset for SnO_2/Ag_2S interface (~0.6 eV) compared with that of ~0.2 eV for TiO_2/Ag_2S, supplied a sufficient injection driving force and was favorable for the electron separation at the heterojunction. When fabricated into solar cells, a dramatically higher current density under AM 1.5 illumination for the SnO_2/Ag_2S heterojunction was obtained, which was contributed by the efficient electron injection.

1. Introduction

Currently, semiconductor sensitized solar cells (SSSCs) have become one of the most popular subjects for research into the next generation of solar cells. Compared with dye sensitized solar cells (DSSCs) which operate using similar principles, semiconductors have outstanding advantages including the photostability of inorganic material, high molar extinction coefficients, tunable energy gaps by controlling the particle size within the quantum dot (QD) region (the as-prepared solar cell is named quantum dot sensitized solar cell, QDSSC), and so on. In recent years, the efficiency of SSSC has improved tremendously, reaching up to about 6% [1–3]. However, the commonly used semiconductors (CdS [4], PbS [5], CdSe [6] and CdTe [7]) contain toxic heavy metals like lead (Pb) or Cadmium (Cd). To develop environment-friendly Pb-free or Cd-free QDs is quite important for consumer-goods applications. Several promising compounds such as Ag_2S [8–10], SnS [11,12], Sb_2S_3 [13], and $CuInS_2$ [14] have attracted the researchers' interest recently. Among them, Ag_2S seems to be a promising candidate with an energy gap of E_g ~1.0 eV [15], which can extend the light absorption to near-infrared spectral regions. Despite this, to the best of our knowledge, there are only three documented attempts [8–10] for fabrication of Ag_2S-sensitized solar cell. Chen [8] and co-workers tried to fabricate Ag_2S solar cell based on TiO_2 nanotubes with a ZnO recombination barrier layer, which exhibited very low photocurrents (the short-circuit current density (J_{sc}) was lower than 1 mA cm^{-2}). Tubtimtae [9] and co-workers have reported a J_{sc} of 7.3 mA cm^{-2} for the optimized Ag_2S-sensitized TiO_2 solar cell accompanied by an efficiency of 0.76%. J. J. Wu and co-workers [10] have fabricated Ag_2S-sensitized ZnO solar cell, obtaining a higher J_{sc} of

* Corresponding author. Tel./fax: +86 10 62772672.
E-mail address: Hong-lin@tsinghua.edu.cn (H. Lin).
[1] These authors contributed equally.

0378-7753/$ – see front matter © 2013 Elsevier B.V. All rights reserved.
http://dx.doi.org/10.1016/j.jpowsour.2013.03.168

13.7 mA cm^{-2}. However, the optimized efficiency was only 0.49%, which mainly resulted from the much lower open-circuit voltage (V_{oc}) of about 100 mV compared with that of the cell based on TiO_2 (about 350 mV).

The underlying issue is why Ag_2S exhibited so poor performance despite its broad absorption spectrum, and whether this can be remedied by proper choice of materials. The answer to this lies in the band alignment between the Ag_2S sensitizer and the oxide electrode. As was known, in SSSC the energy level alignment, especially in the conduction band (CB) between the metal oxide electrode and the sensitizer is vital, and significantly affects the charge separation efficiency at the interface. As calculated from the literature [16], the CB edge of bulk α-Ag_2S is lower in energy by about 0.3 eV than those of the commonly used electrode oxides (TiO_2 and ZnO), which may illustrate that the electron injection from the former into the latter is impossible. However, the significant observed current densities for TiO_2/Ag_2S [9] (7.3 mA cm^{-2}) show that the CB band alignment in an SSSC cannot be simply deduced by extrapolation from bulk values, and call for more detailed experimental observation. Further, it does allude to the fact that an efficient Ag_2S SSSC would require that the anode be composed of an oxide material whose CB is lower in energy, favoring charge separation at the oxide/sensitizer interface [17,18]. One interesting candidate for this purpose is SnO_2, whose conduction band minimum is much lower than those of TiO_2 and ZnO [19–21]. Moreover, the electron mobility of SnO_2 is over 2 orders of magnitude higher than that of TiO_2, which is favorable for the charge transport in the electrode [19]. Here, we chose both TiO_2 and SnO_2 as the semiconductor films to measure the CB offsets in these nanostructured materials. We then tried to fabricate Ag_2S SSSC, expecting higher electron-injection driving force at the Ag_2S/SnO_2 interface and to obtain high current and correspondingly to improve the efficiency. Ag_2S nanoparticles were prepared by the chemical bath deposition (CBD) method. UV–Vis-IR absorption was employed to measure the absorbance and to infer the bandgap. X-ray Photoelectron Spectroscopy (XPS) was used to measure the band alignments at the interface of the heterojunctions. The as-prepared Ag_2S-sensitized photoelectrodes were then fabricated into solar cells whose photovoltaic performances were characterized.

2. Experimental methods

2.1. Solar cell fabrication

SnO_2 electrodes were screen-printed onto FTO glasses with SnO_2 paste prepared by mixing commercial SnO_2 nanoparticles (28%) with terpineol (15%) and a viscous solution of ethyl cellulose in ethanol. The TiO_2 paste was prepared using the similar method. Ag_2S nanoparticless were assembled on the crystallized SnO_2 or TiO_2 electrodes by CBD method as follows. SnO_2 or TiO_2 electrodes were immersed into the solution with 1 mmol $Na_2S_2O_3{\cdot}5H_2O$ and 100 mL 0.05 M silver-ammonia for 4 min at 25 °C. After being washed with deionized water, the electrodes were dried in the air at 70 °C. As a post-treatment, a thin ZnS layer was coated onto the Ag_2S-loaded SnO_2 or TiO_2 electrode. For ZnS deposition, the Ag_2S-sensitized SnO_2 thin films were dipped into an aqueous solution of Zn $(NO_3)_2$ (0.5 M) for 1 min, washed with deionized water thoroughly, dipped again into a methanol solution of Na_2S (0.5 M) for 1 min and at last washed with methanol.

The polysulfide electrolyte consisted of 1 M Na_2S, 1 M S, and 0.1 M NaOH solution in deionized water was utilized. The PbS counter-electrode was prepared by immersing a lead foil into a concentrated H_2SO_4 solution (water: acid volume ratio 1:1) for 24 h at room temperature. Subsequently, the foil was inserted into a polysulfide solution (1 M Na_2S, 0.1 M sulfur, and 0.1 M NaOH dissolved in deionized water) for 24 h, and then rinsed with deionized water and dried in an air stream [29].

2.2. Characterization methods

The crystal structure of Ag_2S was examined on a Bruker D8Advance X-ray diffractometer using Cu Kα radiation (1.5406Å) operating on 40 kV and 40 mA. The sample used for measuring is Ag_2S alone without SnO_2 or TiO_2. High resolution transmission electron microscopy (HRTEM) spectra of Ag_2S QDs were obtained from Tecnai G2 F20 S-Twin (FEI, USA). The absorbance spectra were obtained by an Ultraviolet–visible Spectrophotometer (UV-3310, Shimadzu Co., Japan). As for the sample preparation for absorption measurement, on the one hand, we tried to make the Ag_2S solution as diluted as possible, which will reduce the scattering effect of the Ag_2S nanoparticle. The preparation of the sample is to add 1 mmol $Na_2S_2O_3{\cdot}5H_2O$ into 100 mL 0.05 M silver-ammonia for 4 min (the same time for preparing Ag_2S-sensitized TiO_2 or SnO_2 electrode) at room temperature, which was then diluted for measurement instantly. On the other hand, the diameter of Ag_2S (approximately 5 nm) is relatively small, which enables a transparent solution of Ag_2S dispersed in water [32,33]. X-ray Photoelectron Spectroscopy (XPS) was performed on a PHI Quantera instrument (ULVAC-PHI, Inc. Japan) with Al Ka ($h\nu = 1486.6$ eV) as the X-ray radiation source, which had been carefully calibrated on work function and Fermi energy level (E_f). All XPS spectra were calibrated by the C1s peak at 284.8 eV from contamination to compensate the charge effect. The photovoltaic properties were measured by a computer-controlled digital source meter (Keithley 2400) under AM1.5G radiation from a solar simulator (91192, Oriel; USA) with a black mask. The IMVS/IMPS measurements were performed on a ZAHNER CIMPS system (Zahner, Zahner-Electrik GmbH & Co. KG, Germany) [34]. Stationary as well as sinusoidal modulated light was supplied with a green LED with a maximum wavelength at 546 nm. The light intensity of 200 W m^{-2} was used, under which the V_{oc} and J_{sc} of the solar cell is comparable to those obtained under 100 mW cm^{-2} illuminations (AM 1.5).

3. Results and discussions

As was shown in the XRD pattern (Fig. 1), the Ag_2S nanoparticles have well-defined crystallographic planes and were composed of the monoclinic acanthine in agreement with the PDF card #65-2356, indicating it as α-Ag_2S phase.

The bright field TEM image of Ag_2S deposited SnO_2 nanoparticle is shown in Fig. 2. SnO_2 nanoparticles have diameters ranging from 20 to 40 nm, while the diameter of Ag_2S is approximately 5 nm (also shown in Fig. S1 in Supp. info.). The distribution of Sn, O, Ag and S elemental constituents for Ag_2S deposited SnO_2 nanoparticle is shown by Energy Dispersive Spectroscopy (EDS) (Fig. 2(b)–(e)). Brighter regions indicate higher element content. It was confirmed that Ag_2S nanoparticles were well deposited on the SnO_2 surface.

The optical absorption spectrum of Ag_2S nanoparticles solutions in water is shown in Fig. 3(a), which covered the whole visible and near-infrared region. The value of the optical bandgap for the Ag_2S particles was obtained using the equation for the near-edge absorption and the extrapolation of the linear region of the plot of $(Ahv)^{2/3}$ against photon energy (hv) [16,22] as shown in Fig. 3(b). The absorption corresponds to direct forbidden bandgap of about 1.0 eV, consistent with those reported in the literature [15].

To obtain the conduction band minimum position between Ag_2S and the oxide (TiO_2 or SnO_2), XPS measurements were executed [23,24]. Here we take the SnO_2/Ag_2S system as an example. We first measured the Sn3d and Ag3d core levels $E^{SnO_2}_{Sn3d}$ and $E^{Ag_2S}_{Ag3d}$ as well as

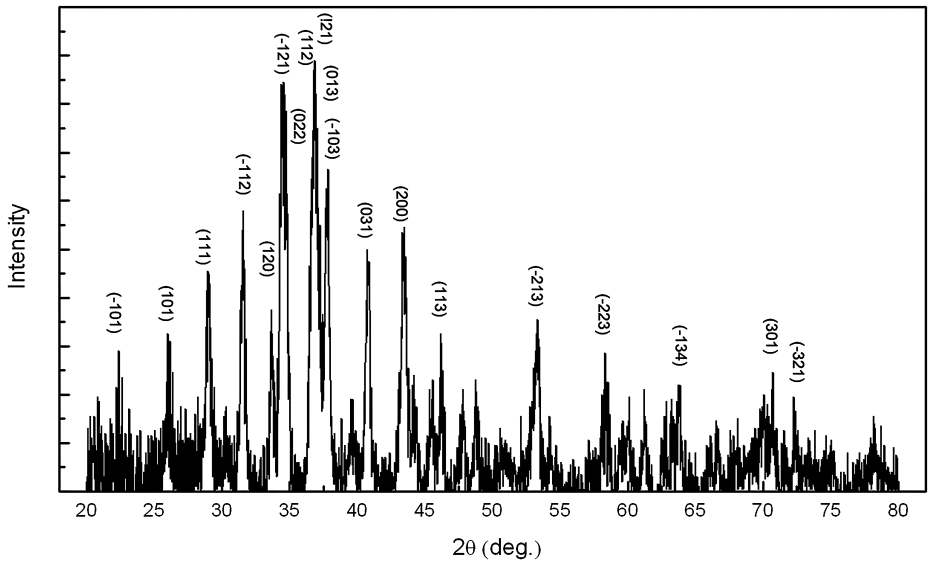

Fig. 1. XRD pattern for the pure Ag_2S (acanthine) nanoparticles without TiO_2 or SnO_2.

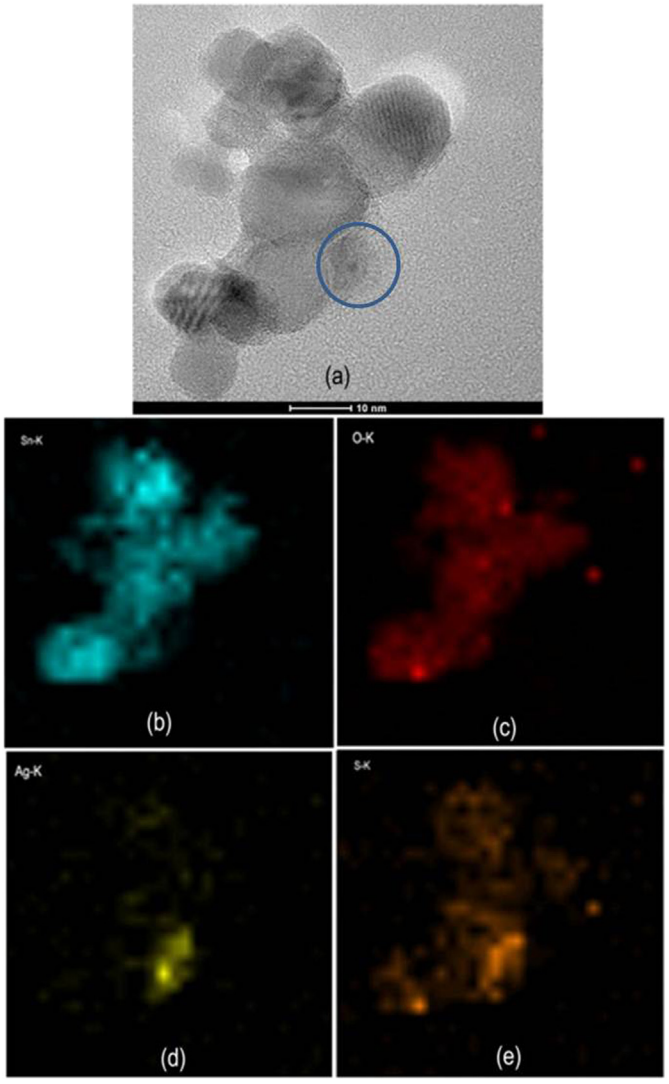

Fig. 2. (a) TEM image of the QDs deposited SnO_2 nanoparticles; (b–e) EDS mapping of the QDs deposited SnO_2 nanoparticles for Sn, O, Ag and S elements, respectively.

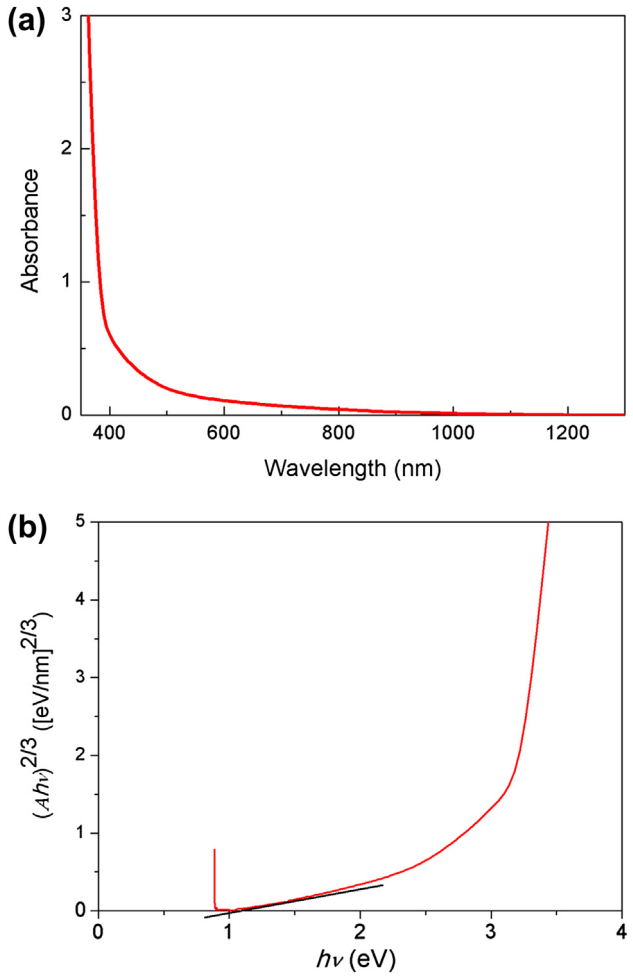

Fig. 3. (a) Optical absorption spectrum of Ag_2S nanoparticles in water. (b) The dependence $(Ahν)^{2/3}$ on the photon energy ($hν$) for Ag_2S nanoparticles using linear extrapolation for the proposed direct forbidden transition.

the valence band maximum (VBM) $E_V^{SnO_2}$ and $E_V^{Ag_2S}$ for SnO_2 and Ag_2S, respectively. These values were measured for the individual films deposited on the FTO glasses. The top of the valence band was determined by linear extrapolation of the leading edge of the valence band of XPS spectra. The relative positions of the Sn 3d and Ag 3d core levels were then determined at the interface of the SnO_2/Ag_2S film. The valence band offset $\Delta E_V^{SnO_2/Ag_2S}$ at the heterojunction interface can be calculated as follows:

$$\Delta E_V^{SnO_2/Ag_2S} = \left(E_{Sn3d}^{SnO_2} - E_V^{SnO_2}\right) - \left(E_{Ag3d}^{Ag_2S} - E_V^{Ag_2S}\right) - \Delta E_{CL}^{SnO_2/Ag_2S} \quad (1)$$

where $\Delta E_{CL}^{SnO_2/Ag_2S}$ is the difference between Sn 3d and Ag 3d at the interface of SnO_2/Ag_2S film. The conduction band discontinuities $\Delta E_C^{SnO_2/Ag_2S}$ can then be calculated from:

$$\Delta E_C^{SnO_2/Ag_2S} = \Delta E_g^{SnO_2/Ag_2S} + \Delta E_V^{SnO_2/Ag_2S} \quad (2)$$

where $\Delta E_g^{SnO_2/Ag_2S}$ represents the difference in energy bandgap between SnO_2 and Ag_2S.

Fig. 4(a) shows the XPS spectra of the SnO_2 thin film, Ag_2S thin film and Ag_2S coated SnO_2 thin film. The characteristic peaks for each element are shown, including the peaks of Sn 3d doublets and Ag 3d doublets. The binding energy value of Sn $3d_{5/2}$ in SnO_2 and Ag $3d_{5/2}$ in Ag_2S were 486.9 eV and 368.3 eV, respectively.

The measured VBM $E_V^{SnO_2}$ of SnO_2 thin film is about 3.5 eV as shown in Fig. 4(b), while the VBM $E_V^{Ag_2S}$ of Ag_2S is about 0.5 eV as shown in Fig. 4(c). Here, the E_g for SnO_2 is taken as 3.6 eV and the value of the direct forbidden bandgap for Ag_2S is taken as 1.0 eV. By substituting those energy values in Eqs. (1) and (2), the valence and conduction band offsets at the interface of the SnO_2/Ag_2S heterojunction are calculated as $\Delta E_V^{SnO_2/Ag_2S} = 3.2$ eV, $\Delta E_C^{SnO_2/Ag_2S} = 0.6$ eV. The same procedures were executed for TiO_2/Ag_2S system. We found that the CB of Ag_2S was about 0.2 eV higher than that of TiO_2 (The detailed XPS spectra of the TiO_2 thin film, Ag_2S thin film and Ag_2S coated TiO_2 thin film are shown in Supp. info). A schematic representation of the band diagram for both systems developed using the energy discontinuities at the heterojunctions is shown in Fig. 5. The CB difference for SnO_2/Ag_2S of 0.6 eV is more than sufficient for the electron separation at the heterojunctions, which should lead to a high J_{sc}.

To confirm the above prediction, we fabricated both the Ag_2S-sensitized SnO_2 and TiO_2 electrodes into solar cells and measured their photovoltaic performance, for which the photocurrent density–voltage (J–V) curves were measured under 100 mW cm^{-2} illuminations (AM 1.5). These are shown in Fig. 6(a), with extracted open-circuit voltage (V_{oc}), short-circuit current density (J_{sc}), fill factor (FF) and conversion efficiency (η) listed in Table 1. Here, PbS was employed as counter-electrode, for which the impressive stability is favorable for Intensity-Modulated Photocurrent/Photovoltage Spectra (IMPS/IMVS) measurements introduced below [25]. It has been observed that J_{sc} for TiO_2 based solar cell is quite low, revealing that 0.2 eV is insufficient for efficient electron injection from the Ag_2S nanoparticle into the anode. It should be also noted that J_{sc} for TiO_2/Ag_2S solar cell in the present work is much lower than that reported in the literature [9], which possibly alludes to the strong dependence of the achievable J_{sc} on the details of Ag_2S preparation methods and processes. However, J_{sc} of about 9 mA cm^{-2} for SnO_2 based solar cell was much higher than that of Ag_2S-sensitized TiO_2 solar cells both in our experiment and described previously in the literature [8,9]. The high current reflects the wide absorption of Ag_2S nanoparticles, but more significantly, should be attributed to the much lower conduction band minimum

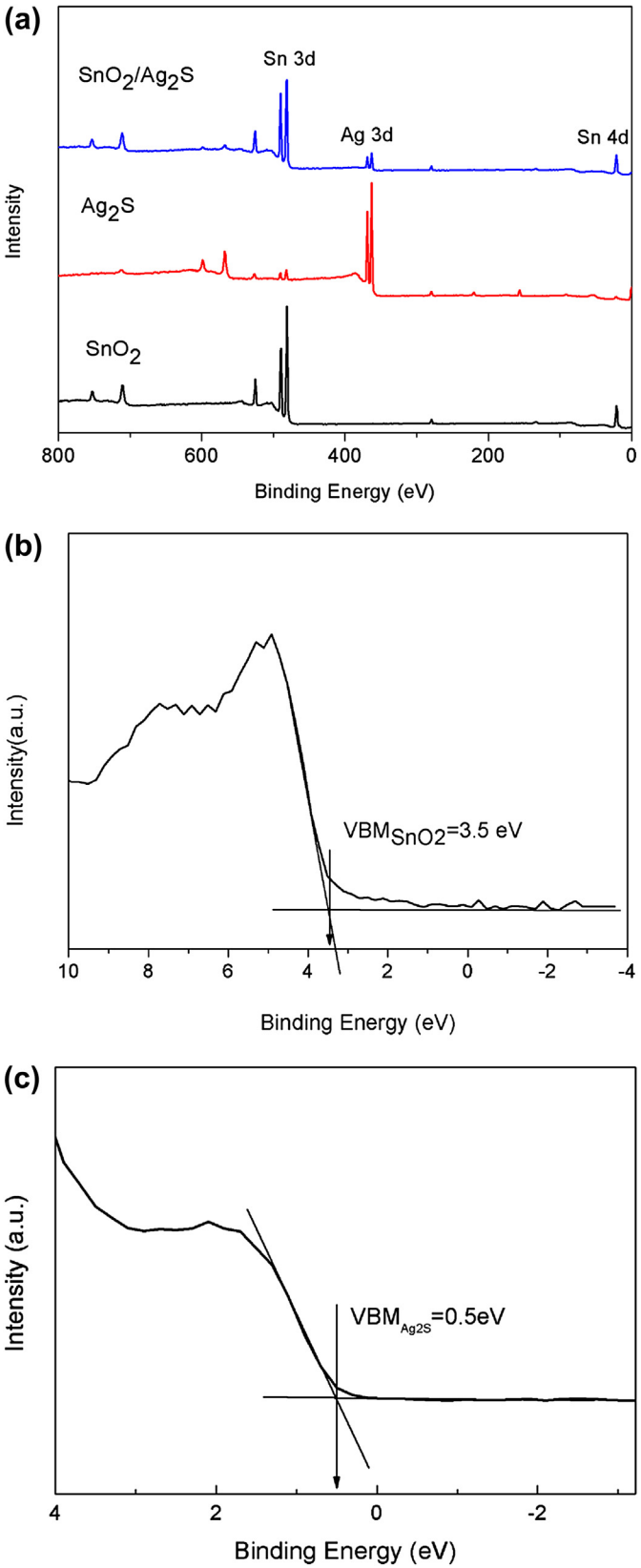

Fig. 4. (a) XPS spectra of the SnO_2 film, Ag_2S thin film and Ag_2S deposited SnO_2 thin film. XPS valence spectrum and the linear interpolation of the leading edge of (b) the SnO_2 film, (c) the Ag_2S films.

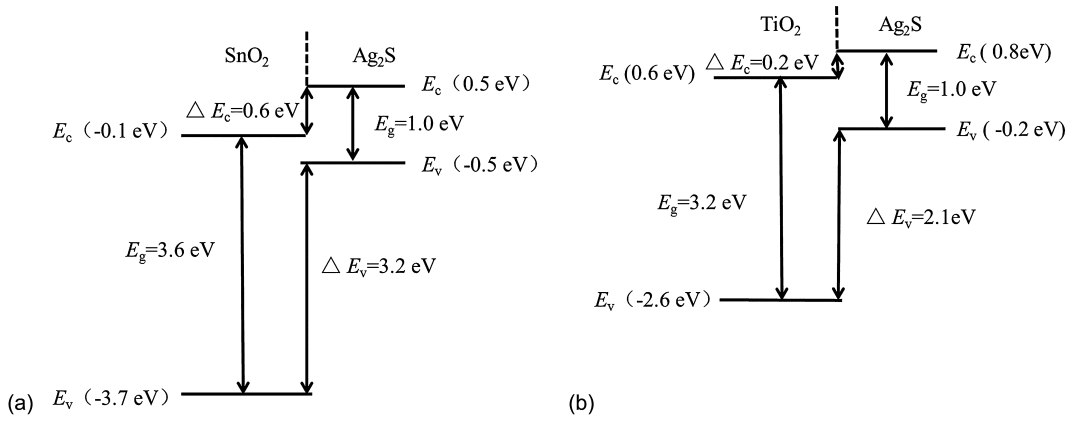

Fig. 5. Energy band diagram of (a) SnO_2/Ag_2S and (b) TiO_2/Ag_2S heterojunction.

of SnO_2 than those of TiO_2 [19–21]. Correspondingly, the solar cell efficiency of 0.41% based on SnO_2/Ag_2S was much higher than that based on TiO_2/Ag_2S.

IPCE spectra (Fig. 6(b)) show coverage of the whole visible spectrum and the NIR spectrum till ~1000 nm, proving that Ag_2S can serve as a wide spectral absorption sensitizer candidate. The wavelength-dependent IPCE is given by:

$$\mathrm{IPCE}(\lambda) = \mathrm{LHE}(\lambda) \times \eta_{\mathrm{inj}} \times \eta_{\mathrm{c}} \tag{3}$$

where LHE is the light harvesting efficiency at a given wavelength, η_{inj} is the electron-injection efficiency, and η_{c} is the charge collection efficiency. As was discussed above, the much lower IPCE for TiO_2 based solar cell is mainly due to the insufficient electron-injection driving force. Further, η_{c}, which also affects the IPCE yielding largely determined by the recombination in the solar cell, was shown as follows:

$$\eta_{\mathrm{c}} = J_{\mathrm{sc}}/J_{\mathrm{inj}} = J_{\mathrm{sc}}/(J_{\mathrm{sc}} + J_{\mathrm{r}}) = 1 - \tau_{\mathrm{c}}/\tau_{\mathrm{n}} \tag{4}$$

where J_{inj} and J_{r} are the electron-injection current density from QD to the photoanode and the recombination current density respectively, while τ_{n} represents the electron lifetime and τ_{c} is the electron collection lifetime.[26] η_{c} was evaluated below to disclose the origin of the low FF for the solar cells, which may be resulted from the high recombination loss revealed in DSSCs [27].

IMPS/IMVS [28–31] measurement was carried out to gain information into the kinetic electron transfer processes and reveal the recombination loss in the solar cells. Briefly, IMPS measures the periodic photocurrent response of a testing cell to a small sinusoidal perturbation of the light intensity superimposed on a larger steady background level, providing information on charge transport and back reaction under short-circuit conditions. IMVS experiment uses the same intensity perturbation but measures the periodic modulation of the photovoltage, detailing the dynamics of τ_{n} under open-circuit conditions. Experimentally, τ_{n} and τ_{c} were estimated from both the IMVS response of $\tau_{\mathrm{n}} = 1/2\pi f_{\mathrm{min(IMVS)}}$ (where $f_{\mathrm{min(IMVS)}}$ is the characteristic frequency minimum of the IMVS imaginary component) and the IMPS response using $\tau_{\mathrm{c}} = 1/2\pi f_{\mathrm{min(IMPS)}}$ (where $f_{\mathrm{min(IMPS)}}$ is the characteristic frequency minimum of the IMPS imaginary component), respectively.

As was shown in Table 1, τ_{c} in SnO_2 based solar cells is much smaller than that in TiO_2 based one, which is in agreement with the better charge transport properties in the SnO_2 film [19]. Meanwhile, the obviously smaller τ_{n} for SnO_2 based solar cell reveals more serious recombination. To figure out the origin of this recombination, SnO_2 and TiO_2 film morphology were observed by SEM (shown in Supp. info.). Severe cracks were observed even under very low magnification for SnO_2, which are probably detrimental to the electron transport and act as electron recombination channels.

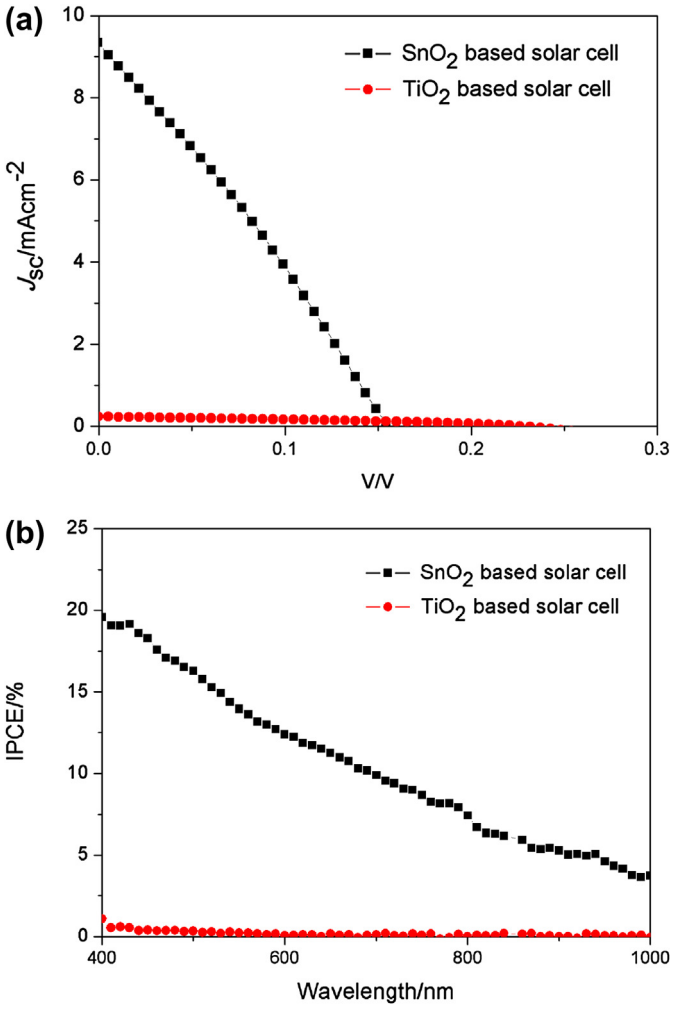

Fig. 6. Current density vs. voltage (a) and IPCE curves (b) for Ag_2S semiconductor sensitized solar cells based on SnO_2 and TiO_2 as was measured under 1 sun of simulated irradiation (AM1.5G, 100 mW/cm^2). PbS counter-electrode was used.

Table 1
Open-circuit voltage (V_{OC}), short-circuit current density (J_{SC}), fill factor (FF), and the total cell efficiency (η) from Fig. 6(a), and electron collection lifetime (τ_c), electron lifetime (τ_n) and charge collection efficiency (η_{col}) calculated from the IMPS & IMVS measurement.

Oxides	V_{OC}/mV	J_{SC}/mA cm^{-2}	FF	E_{ff}/%	$f_{min(IMPS)}$	τ_c/s	$f_{min(IMVS)}$	τ_n/s	η_{col}
SnO_2	154	9.04	0.295	0.41	2.969	0.0536	0.5523	0.288	81.4%
TiO_2	226	0.24	0.350	0.019	1.065	0.150	0.1433	1.111	86.5%

Overall, the charge collection efficiency for SnO_2/Ag_2S system is about 80% under 200W m^{-1} [2] illumination, which could be enhanced by preparation process optimization of SnO_2 paste with better printable properties and is now underway in our lab.

It should also been noted that V_{oc} of Ag_2S-sensitized solar cell, which is determined by the difference between the quasi Fermi level of the electrons in SnO_2 under illumination and the redox potential of the electrolyte [20], was also low. Since the redox potential of the electrolyte should be higher than the valence band of Ag_2S for the sensitizer's regeneration, the maximum achievable V_{oc} should be less than 0.4 eV for SnO_2/Ag_2S system, inferred from the difference between the conduction band of SnO_2 and the valence band of Ag_2S. The V_{oc} yield for the TiO_2/Ag_2S is larger due to the higher conduction band of TiO_2 than that of SnO_2. Thus the need to find, for this system, an anode material with a smaller CB offset, but one not as large as SnO_2, and not as small as TiO_2 is necessary in order to optimize the Ag_2S-sensitized solar cell by keeping a balance between J_{sc} and V_{oc}. Semiconductors such as Nb_2O_5 and $BaTiO_3$ may be potential candidates [16].

4. Conclusion

In summary, an in-situ study of the CB band offsets in the nanostructured Ag_2S-sensitized electrodes has been presented, from which the results were different from the extrapolated bulk values. The larger CB difference at SnO_2/Ag_2S interface than that of TiO_2/Ag_2S due to the lower CB minimum of SnO_2 vs. TiO_2 facilitates charge carrier separation at the heterojunction interface. This was proved by the impressive J_{sc} for SnO_2/Ag_2S system, which was not only obviously higher than that fabricated for Ag_2S/TiO_2 system in our group but also than that reported in the literature. Further improvement of the photovoltaic performance of Ag_2S SSSC are expected by selecting anode materials with more suitable band position and by preparing more uniform SnO_2 films to reduce the recombination.

Acknowledgments

The authors express their gratitude for the support provided by the MOST international S&T cooperation program of China (2010DFA64360), the Ministry of Science & Technology, Israel and the Ministry of Science & Technology, P.R. China: the China–Israel Scientific and Strategic Research Fund-No. 7 of the 5th round, and the National Natural Science Foundation of China (NSFC, 51272126).

Appendix A. Supporting information

Supplementary data related to this article can be found at http://dx.doi.org/10.1016/j.jpowsour.2013.03.168.

References

[1] S. Ruhle, M. Shalom, A. Zaban, ChemPhysChem 11 (2010) 2290.
[2] Z.S. Yang, C.Y. Chen, P. Roy, H.T. Chang, Chem. Commun. 47 (2011) 9561.
[3] J.H. Im, C.R. Lee, J.W. Lee, S.W. Park, N.G. Park, Nanoscale 3 (2011) 4088.
[4] L.M. Peter, D.J. Riley, E.J. Tull, K.G.U. Wijayantha, Chem. Commun. 10 (2002) 1030.
[5] J.M. Luther, J.B. Gao, M.T. Lloyd, O.E. Semonin, M.C. Beard, A.J. Nozik, Adv. Mater. 22 (2010) 3704.
[6] I. Mora-Sero, J. Bisquert, T. Dittrich, A. Belaidi, A.S. Susha, A.L. Rogach, J. Phys. Chem. C 111 (2007) 14889.
[7] I. Mora-Sero, D. Gross, T. Mittereder, A.A. Lutich, A.S. Susha, T. Dittrich, A. Belaidi, R. Caballero, F. Langa, J. Bisquert, A.L. Rogach, Small 6 (2010) 221.
[8] C. Chen, Y. Xie, G. Ali, S.H. Yoo, S.O. Cho, Nanoscale Res. Lett. 6 (2011) 462.
[9] A. Tubtimtae, K.L. Wu, H.Y. Tung, M.W. Lee, G.J. Wang, Electrochem. Commun. 12 (2010) 1158.
[10] J.J. Wu, R.C. Chang, D.W. Chen, C.T. Wu, Nanoscale 4 (2012) 1368.
[11] H.T. Liu, Y. Liu, Z. Wang, P. He, Nanotechnology 21 (2010) 105707.
[12] Y. Xu, N. Al-Salim, C.W. Bumby, R.D. Tilley, J. Am. Chem. Soc. 131 (2009) 15990.
[13] Y. Itzhaik, O. Niitsoo, M. Page, G. Hodes, J. Phys. Chem. C 113 (2009) 4254.
[14] K.T. Kuo, D.M. Liu, S.Y. Chen, C.C. Lin, J. Mater. Chem. 19 (2009) 6780.
[15] A.N. Rodrıguez, M.T.S. Nair, P.K. Nair, Semicond. Sci. Technol. 20 (2005) 576.
[16] Y. Xu, M.A.A. Schoonen, Am. Mineral. 85 (2000) 543.
[17] H.C. Leventis, F. O'Mahony, J. Akhtar, M. Afzaal, P. O'Brien, S.A. Haque, J. Am. Chem. Soc. 132 (2010) 2743.
[18] J.J.H. Pijpers, R. Koole, W.H. Evers, A.J. Houtepen, S. Boehme, C.D.M. Donega, D. Vanmaekelbergh, M. Bonn, J. Phys. Chem. C 114 (2010) 18866.
[19] M.A. Hossain, J.R. Jennings, Z.Y. Koh, Q. Wang, ACS Nano 5 (2011) 3172.
[20] A. Kay, M. Graetzel, Chem. Mater. 14 (2002) 2930.
[21] J.J. Ning, K.K. Men, G.J. Xiao, L. Wang, Q.Q. Dai, B. Zou, B.B. Liu, G.T. Zou, Nanoscale 2 (2010) 1699.
[22] A. Hagfeldt, M. Graetzel, Chem. Rev. 95 (1995) 49.
[23] A.M. Haleem, M. Ichimura, J. Appl. Phys. 107 (2010) 034507.
[24] C.H. Jia, Y.H. Chen, Y. Guo, X.L. Liu, S.Y. Yang, W.F. Zhang, Z.G. Wang, Nanoscale Res. Lett. 6 (2011) 316.
[25] Z. Tachan, M. Shalom, I. Hod, S. Reuhle, S. Tirosh, A. Zaban, J. Phys. Chem. C 115 (2011) 6162.
[26] K. Zhu, T.B. Vinzant, N.R. Neale, A.J. Frank, Nano Lett. 7 (2007) 3739.
[27] A.N.M. Green, E. Palomares, S.A. Haque, J.M. Kroon, J.R. Durrant, J. Phys. Chem. B 109 (2005) 12525.
[28] G. Schlichthorl, N.G. Park, A.J. Frank, J. Phys. Chem. B 103 (1999) 782.
[29] N.G. Park, G. Schlichthorl, J.V.D. Lagemaat, H.M. Cheong, A. Mascarenhas, A.J. Frank, J. Phys. Chem. B 103 (1999) 3308.
[30] L. Dloczik, O. Ileperuma, I. Lauermann, L.M. Peter, E.A. Ponomarev, G. Redmond, N.J. Shaw, I. Uhlendorf, J. Phys. Chem. B 101 (1997) 10281.
[31] J.V. D Lagemaat, A.J. Frank, J. Phys. Chem. B 104 (2000) 4292.
[32] Z.T. Deng, D.R. Han, Y. Liu, Nanoscale 3 (2011) 4346.
[33] S.G. Hickey, C. Waurisch, B. Rellinghaus, A. Eychmuller, J. Am. Chem. Soc. 130 (2008) 14978.
[34] F. Hao, X. Wang, C. Zhou, X.J. Jiao, X. Li, J.B. Li, H. Lin, J. Phys. Chem. C 116 (2012) 19164.